

## Indium phosphide-based monolithically integrated PIN waveguide photodiode readout for resonant cantilever sensors

N. P. Siwak, X. Z. Fan, S. Kanakaraju, C. J. K. Richardson, and R. Ghodssi

Citation: [Applied Physics Letters](#) **105**, 143102 (2014); doi: 10.1063/1.4897276

View online: <http://dx.doi.org/10.1063/1.4897276>

View Table of Contents: <http://scitation.aip.org/content/aip/journal/apl/105/14?ver=pdfcov>

Published by the [AIP Publishing](#)

---

### Articles you may be interested in

[Waveguide-integrated photonic crystal spectrometer with camera readout](#)

*Appl. Phys. Lett.* **105**, 051103 (2014); 10.1063/1.4892265

[Polymeric cantilever-based biosensors with integrated readout](#)

*Appl. Phys. Lett.* **89**, 173505 (2006); 10.1063/1.2364843

[Subpicosecond high-power mode locking using flared waveguide monolithic quantum-dot lasers](#)

*Appl. Phys. Lett.* **88**, 133119 (2006); 10.1063/1.2186110

[Monolithic integration of resonant tunneling diodes and heterojunction bipolar transistors on patterned InP substrates](#)

*J. Vac. Sci. Technol. B* **16**, 1413 (1998); 10.1116/1.589957

[High-frequency behavior of waveguide integrated photodiodes monolithically integrated on InP using optical butt coupling](#)

*J. Appl. Phys.* **81**, 2511 (1997); 10.1063/1.363959

---

The logo for AIP Chaos is centered on a dark red background with a subtle geometric pattern. The letters 'AIP' are in a large, white, sans-serif font, followed by a vertical orange bar and the word 'Chaos' in a smaller, white, sans-serif font.

AIP | Chaos

**CALL FOR APPLICANTS**  
Seeking new Editor-in-Chief

## Indium phosphide-based monolithically integrated PIN waveguide photodiode readout for resonant cantilever sensors

N. P. Siwak,<sup>1,2</sup> X. Z. Fan,<sup>1</sup> S. Kanakaraju,<sup>2</sup> C. J. K. Richardson,<sup>2</sup> and R. Ghodssi<sup>1</sup>

<sup>1</sup>Department of Electrical and Computer Engineering, Institute for Systems Research, University of Maryland, College Park, Maryland 20742, USA

<sup>2</sup>Laboratory for the Physical Sciences, 8050 Greenmead Drive, College Park, Maryland 20740, USA

(Received 8 July 2014; accepted 23 September 2014; published online 6 October 2014)

An integrated photodiode displacement readout scheme for a microelectromechanical cantilever waveguide resonator sensing platform is presented. III-V semiconductors are used to enable the monolithic integration of passive waveguides with active optical components. This work builds upon previously demonstrated results by measuring the displacement of cantilever waveguide resonators with on-chip waveguide PIN photodiodes. The on-chip integration of the readout provides an additional 70% improvement in mass sensitivity compared to off-chip photodetector designs due to measurement stability and minimized coupling loss. In addition to increased measurement stability, reduced packaging complexity is achieved due to the simplicity of the readout design. We have fabricated cantilever waveguides with integrated photodetectors and experimentally characterized these cantilever sensors with monolithically integrated PIN photodiodes. © 2014 AIP Publishing LLC. [<http://dx.doi.org/10.1063/1.4897276>]

Resonant cantilevers are well established as a sensor transduction method. Cantilevers are coated with a receptor material that absorbs specific chemical or biological species and the attachment of these species changes the mass of the cantilever, shifting the cantilever's resonant frequency. Masses on the order of attograms have been measured with this type of device.<sup>1</sup> Cantilever sensors exhibiting this high sensitivity are generally measured using external optical techniques.<sup>2-4</sup> The most common and sensitive method is similar to that employed in atomic force microscopy (AFM) where a laser is reflected off the cantilever surface onto a position sensitive detector. Oscillations of the cantilever can be measured by monitoring the continuously changing response of the detector.<sup>5</sup> Other optical methods, such as interferometric measurements,<sup>6,7</sup> can be used to achieve ultra-sensitive displacement resolution; however, like AFM techniques, they generally require costly equipment and infrastructure which cannot be easily integrated. The major drawback in using optical readout methods lies in the large free-space optical components (lasers, alignment mirrors, etc.) required, which limit the transition of these sensors from laboratory use to portable systems. Alignment tolerance and accuracy also necessitate larger cantilevers, which can decrease the effectiveness of these sensors.<sup>8,9</sup> Non-optical methods, such as piezoelectric, piezoresistive, and capacitive readout schemes, have also been employed to measure cantilever response;<sup>4</sup> however, they do not offer the same benefits of high displacement sensitivity and relative noise immunity that optical methods exhibit. The development of sensitive, compact, and portable sensors may be benefited by using a different readout approach.

The sensor readout architecture presented here uses a traditional cantilever sensor platform with an in-plane, optical approach using suspended Indium Phosphide (InP) cantilever waveguides to couple light into an on-chip waveguide PIN photodiode. This readout scheme is based upon the modulation of optical coupling between a free air-cladded

cantilever waveguide and a fixed output waveguide coupled to a photodiode.<sup>10-13</sup> An illustration of the readout concept is shown in Figure 1. Optical power is coupled onto chip and passed through the input waveguide. The cantilevers are actuated electrostatically by applying a voltage between the cantilever and a parallel actuation electrode. Displacement changes the amount of optical power that is coupled into the output waveguide and photodiode from the input waveguide. This configuration reduces alignment requirements by using lithographical patterning to align components rather than free-space optics. Furthermore, this demonstration integrates the output optical power measurement on-chip and eliminates much of the optical readout support equipment needed in previous demonstrations.<sup>14</sup> These sensors demonstrate high displacement sensitivity (nm-level) such as is obtained with traditional optical readout techniques. Additionally, III-V materials are attractive for this application due to the adjustable bandgap properties, allowing for active and passive optical devices to be designed within the same substrate.

The integrated PIN photodiode is constructed from the layer structure as shown in Figure 2. The device uses the p-type region as a waveguide, the sacrificial InGaAs layer as

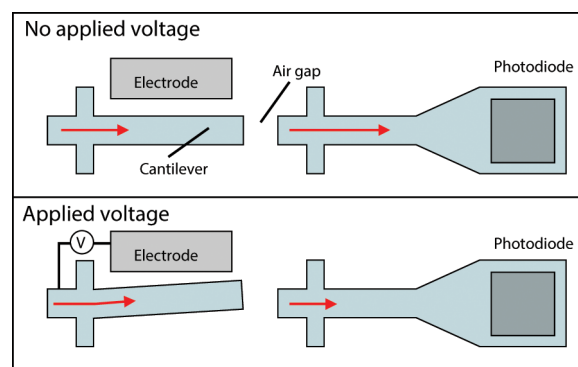


FIG. 1. Illustration of cantilever actuation causing variation in coupling of light due to misalignment of waveguide.

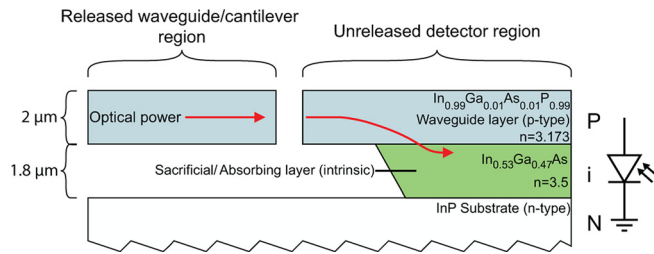


FIG. 2. Schematic of photodetector operation and layer structure detail.

the intrinsic photoabsorbing layer, and the substrate as the n-type region. Waveguides are tapered to a wide width that allows for InGaAs to remain below after the undercut of the narrow sections of the waveguide (see Figure 3). Light couples from the lower index waveguide ( $n = 3.1$ ) into the higher index ( $n = 3.5$ ) InGaAs layer due to this index contrast. Reverse biasing this structure allows it to operate in the photoconducting mode. Actuating the cantilever resonator with a voltage impulse allows the resonant frequency to be determined by taking the Fourier transform of the resulting optical signal. Monitoring the resonant frequency allows mass changes to be discerned by using a well-established relationship between resonant frequency and mass, described by Lavrik *et al.*<sup>4</sup>

The projected mass sensitivity of the cantilever resonator can be shown to be related to the resonant frequency of the device. Mass loading sensitivity can be expressed as<sup>4</sup>

$$\frac{\Delta m}{\Delta f} = \frac{0.48 \cdot m_o}{f_o c_A}, \quad (1)$$

where  $m_o$  is the cantilever mass,  $f_o$  is the resonant frequency, and  $c_A$  is a coefficient from 0.24 to 1 describing the distribution of the mass absorbed (1 = concentrated at the cantilever tip). From (1), we observe that the sensitivity is inversely proportional to the resonant frequency of the cantilever. The quality factor ( $Q$ ) of high frequency resonators are also

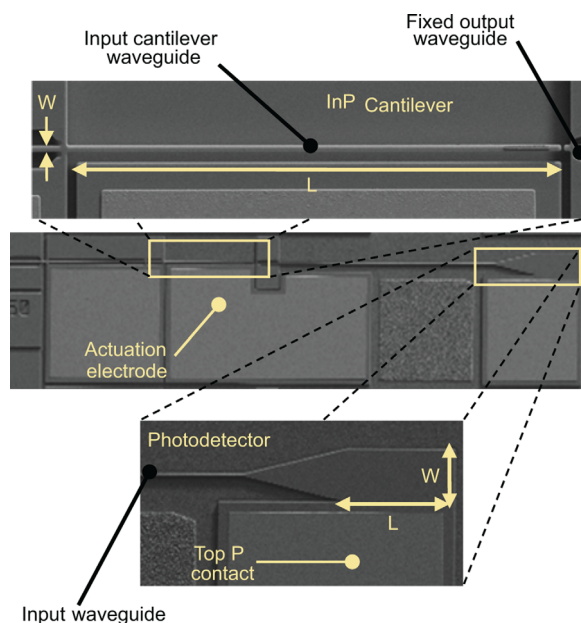


FIG. 3. Scanning electron micrograph showing InP resonators with integrated photodetectors. Above image magnified to show cantilever and detector dimensions.

raised,<sup>15</sup> increasing the resolution to which  $\Delta f$  can be measured, further enhancing the sensitivity.

Waveguide PIN photodiodes are modeled using the COMSOL Multi-physics finite element analysis software package to simulate 1550 nm optical propagation and absorption through the structure. It is expected that absorption from waveguide into the absorbing layer (InGaAs) will be resonant in nature and dependent on its thicknesses.<sup>16</sup> A two dimensional model of our structure was constructed (see Figure 2) with the assumption that that absorption in the InGaAs layer would be the dominant loss mechanism. Absorption was modeled as resistive heating in the COMSOL simulations. As the layer becomes thicker, periodic absorption becomes less pronounced due to the increased density of modes. Choosing a thickness of 1.8  $\mu\text{m}$  for the InGaAs layer places absorption at a peak point and reduces the sensitivity to thickness variations by operating near a thickness-insensitive regime. Final photodiode structures are designed with waveguide widths of 25–55  $\mu\text{m}$ , and lengths of 25–100  $\mu\text{m}$  in order to characterize the limitations of the photodiodes empirically.

The cantilever waveguide sensors with integrated photodiodes are fabricated based on tethered suspended waveguides in photonic materials such as InP, first demonstrated in Refs. 11 and 17. Readers are encouraged to see these papers for more detailed information about design and fabrication. The details presented here include modifications made to facilitate the fabrication of an integrated PIN photodiode. Devices are fabricated from an in-house molecular beam epitaxy (MBE) epitaxial growth (Figure 2). Each layer is grown lattice matched on an InP:Fe wafer. This allows fabrication of waveguides from mechanically and optically superior materials. InGaAs is grown as a sacrificial layer as it can be selectively removed from InP. The mole fractions in the waveguiding layer (InGaAsP) are added to induce tensile stress in order to prevent suspended waveguides (doubly clamped beams) from buckling. Three inch wafers are then cut into 18  $\times$  18 mm<sup>2</sup> die for further processing.

This die is then coated with 7000  $\text{\AA}$  of SiO<sub>2</sub> as an etch mask. A 5 $\times$  projection lithography system was used to pattern the waveguide features in photoresist which are then transferred into the oxide using a CHF<sub>3</sub>/O<sub>2</sub> dry etch. Waveguide features are etched using a cyclic H<sub>2</sub>-CH<sub>4</sub>, and O<sub>2</sub> etching process described in Ref. 18 that achieves highly vertical sidewalls (89°) and low surface roughness (20 nm). Top metal contacts of Ti-Pt-Au are deposited to make contact to the p-type waveguide layer. A second metal layer of Ni-Au-Ge-Ni-Au is deposited on the backside and annealed at 300–400 °C to create ohmic contacts to the n-type InP layer. A H<sub>3</sub>PO<sub>4</sub>:H<sub>2</sub>O<sub>2</sub>:H<sub>2</sub>O (1:1:8) wet etch is used to remove the sacrificial InGaAs layer preferentially from the InGaAsP. Increased widths of photodetector regions are designed to prevent total undercut and release during this stage. CO<sub>2</sub> critical point drying is used as a final step to prevent waveguide stiction. A scanning electron micrograph of the finished device is shown in Figure 3.

The experimental setup for the cantilever waveguide resonator with integrated photodiodes is simplified compared to previous design iterations. A block diagram of the setup is shown in Figure 4. Optical input to the cantilever waveguide is provided via a tunable laser at the wavelength of 1550 nm,

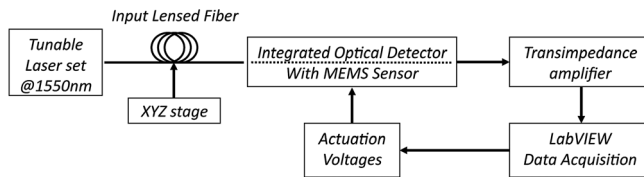


FIG. 4. Block diagram of measurement setup.

coupled to the microelectromechanical (MEMS) device through a lensed fiber. The photodiode is reverse biased at  $-1$  V and the output signal from the integrated photodiode is fed into an oscilloscope through a transimpedance amplifier. The cantilever actuation voltage is provided directly from a function generator. Since no physical electrical isolation exists across the various components, all electrodes are maintained at a lower potential than the substrate to assure a reverse bias of all junctions beneath the contacts. The tunable laser was set at the maximum output power of 8 mW. Measurement of the PIN photodiodes alone yielded an average responsivity of 0.25 A/W, shunt resistance of 600 k $\Omega$ , and a series resistance of 6 k $\Omega$ . Maximum photocurrent was measured to be 30  $\mu$ A and the dark current at  $-1$  V reverse bias was shown to be less than 1 nA. Analysis of the dark current variation versus photodiode size as per Ref. 19 indicates that the limitations of this design are leakage currents primarily to surface states rather than bulk defects. From the photodiode responsivity, we estimate that 0.12 mW of optical power is absorbed by the detector. This yields a total loss of  $-20$  dB from source-to-detector, attributed to primarily coupling loss due to mode mismatch, as well as waveguide and fiber propagation losses.

The cantilever's resonant frequency is measured with a pulsed ring-down technique. A 30 V DC bias is placed across the cantilever and actuator electrodes, providing a steady state cantilever displacement due to electrostatic actuation and also serving to reverse bias the PIN junction and prevent parasitic current flow. An inverted square pulse actuation signal at 3 kHz is applied to the cantilever electrode, causing it to oscillate and decay to a rest position during the minimum of the square pulse signal. Its resonant frequency is then determined with a Fourier transform and Lorentzian fit. The minimum of the actuation pulse is set at 10 V, maintaining the reverse bias of the PIN junction. This applied bias during ring down will induce a frequency shift proportional to the applied voltage due to the energy that is stored within the capacitor made up of the cantilever and actuation electrode, effectively increasing the cantilever's spring constant.<sup>14</sup> Up to 10 kHz of frequency tuning was observed at 30 V of applied bias for the 50  $\mu$ m long cantilever presented here. The cutoff frequency of the photodiode is influenced by the transit time of the carriers across the intrinsic absorbing region and the RC time constant of the diode consisting of the series resistance and junction capacitance. A cutoff frequency of 2.1 GHz is calculated due to the transit time of the carriers, and a cutoff frequency of 110 MHz is calculated due to the RC time constant. Both of these values are far beyond the operating range of the integrated cantilevers, and thus should pose no physical limitation on the operation due to cutoff frequencies.

Using the integrated photodetector with the data acquisition setup, the resonant frequency of this device was measured to be 282.3 kHz  $\pm$  24 Hz over 20 min of data acquisition. The device response is shown in Figure 5, and a Fourier transform of the displacement signal in Figure 6. From the Fourier transform, we estimate a signal to noise ratio of 18 dB for these measurements. Using Eq. (1) and estimating a minimum  $\Delta f$  from the frequency uncertainty, this particular sensor has the potential to measure a minimum  $\Delta m$  of  $16.7 \times 10^{-15}$  g.

In this experiment, we have observed an improvement of run-to-run measurement stability over the discrete photodiode measurement technique. The cantilever frequency measurements with the integrated photodiodes show a standard deviation of  $\pm 24$  Hz over a 20 min measurement period, while previously reported external photodiode methods exhibit a standard deviation of  $\pm 100$  Hz for the same sampling period.<sup>12</sup> For both cases, signal-to-noise ratios are comparable (17 dB for the off-chip detector and 18 dB for the integrated detector), and thus this measurement of the resonant frequency is not likely impacted by the signal quality, but rather, instrumentation limitations.

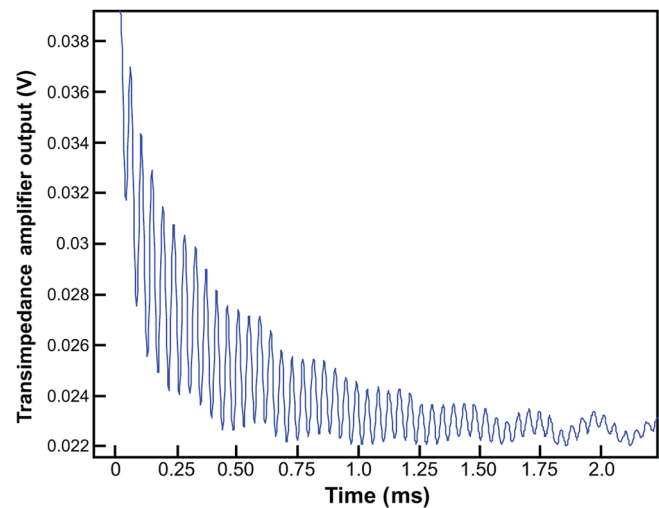


FIG. 5. Underdamped response of cantilever due to step voltage actuation.

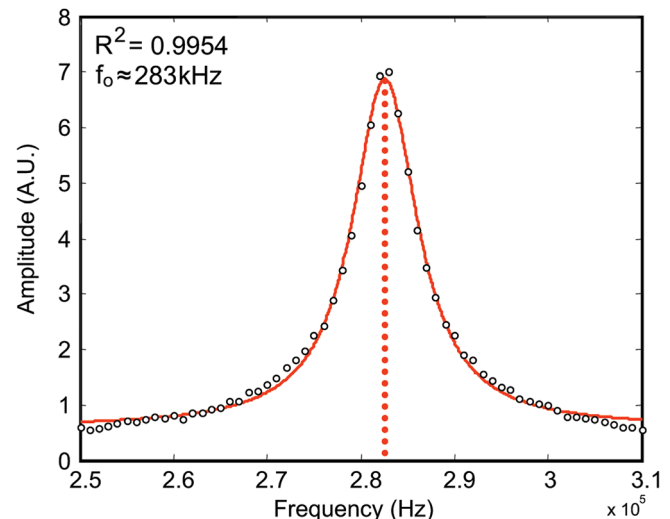


FIG. 6. Lorentzian fit to the Fourier transform of underdamped response due to step voltage actuation.

Significant changes in optical coupling and frequency measurement are the major contributors to the noise and uncertainty seen in our results. Mechanical drift of the input fiber on the electrostrictive stages is not constant and depends on environmental factors such as temperature and humidity and contributes to reduction in coupled power. Leakage currents through the actuation electrodes that are not electrically isolated from the photodiode can be incorrectly interpreted as mechanical movement. Finally, a non-ideal testing environment (ambient vibrations, air currents, etc.) creates unpredictable changes in the coupled optical power. The PIN photodiodes fabricated here had no surface passivation treatments applied, and the defect density in the depletion region is unknown. These defects introduce additional current paths in parallel with the photodiode, which contributes to the lower shunt resistance observed and thus greater noise in the photocurrent. Analysis shows that a significant portion of leakage current arises at the surface of the photodiode; thus performing a surface passivation step may reduce the leakage current. Responsivity of these photodiodes can be improved by reducing the parasitic resistances in the metal contact regions and improved material quality. The mass resolution of these devices can be increased in future designs with shorter cantilevers to obtain higher resonant frequencies and therefore improved sensitivity.

We have presented the design, fabrication, and testing of a cantilever waveguide resonant sensor with an integrated PIN waveguide photodiode. Photodiodes with a cutoff frequency of 110 MHz and responsivities of 0.25 A/W were fabricated and characterized. The measurement uncertainty using these devices has been compared with previous cantilever waveguide sensor designs, showing an improvement in mass resolution of approximately  $4.0 \times 10^{-14}$  g due to the reduced impact of non-ideal instrumentation on the integrated system. Fabricating these sensors in III-V materials is a key demonstration of this technology as it provides the building blocks for further development of these stand-alone sensor platforms. Monolithically integrating optical sources with the passive waveguides and photodiodes will further ease sensor implementation and eliminate need for external measurement equipment. Future designs will provide additional electrical isolation between device components, higher device sensitivities due to geometry optimization of both cantilevers and photodiodes, and ultimately monolithically integrated optical sources to facilitate readout without fiber-to-chip coupling losses associated with lensed fibers and unstable instrumentation.

This work was supported by a National Science Foundation CAREER Award and the Laboratory for Physical Sciences (LPS). The authors would like to thank J.

McGee for advice in relation to data analysis, D. Hinkel, W. Berk, S. Horst, and L. Olver at the Laboratory for Physical Sciences for facility access and processing assistance.

- <sup>1</sup>B. Ilic, H. G. Craighead, S. Krylov, W. Senaratne, C. Ober, and P. Neuzil, "Attogram detection using nanoelectromechanical oscillators," *J. Appl. Phys.* **95**(7), 3694–3703 (2004).
- <sup>2</sup>N. V. Lavrik and P. G. Datskos, "Femtogram mass detection using photo-thermally actuated nanomechanical resonators," *Appl. Phys. Lett.* **82**(16), 2697 (2003).
- <sup>3</sup>B. Ilic, D. Czaplewski, M. Zalalutdinov, H. G. Craighead, P. Neuzil, C. Campagnolo, and C. Batt, "Single cell detection with micromechanical oscillators," *J. Vac. Sci. Technol., B* **19**(6), 2825 (2001).
- <sup>4</sup>N. V. Lavrik, M. J. Sepaniak, and P. G. Datskos, "Cantilever transducers as a platform for chemical and biological sensors," *Rev. Sci. Instrum.* **75**(7), 2229 (2004).
- <sup>5</sup>L. A. Pinnaduwa, D. L. Hedden, A. Gehl, V. I. Boiadjev, J. E. Hawk, R. H. Farahi, T. Thundat, E. J. Houser, S. Stepnowski, R. A. McGill, L. Deel, and R. T. Lareau, "A sensitive, handheld vapor sensor based on microcantilevers," *Rev. Sci. Instrum.* **75**(11), 4554 (2004).
- <sup>6</sup>B. R. Ilic, S. Krylov, M. Kondratovich, and H. G. Craighead, "Optically actuated nanoelectromechanical oscillators," *IEEE J. Sel. Top. Quantum Electron.* **13**(2), 392–399 (2007).
- <sup>7</sup>B. Ilic, S. Krylov, and H. G. Craighead, "Theoretical and experimental investigation of optically driven nanoelectromechanical oscillators," *J. Appl. Phys.* **107**(3), 034311 (2010).
- <sup>8</sup>K. L. Ekinici and M. L. Roukes, "Nanoelectromechanical systems," *Rev. Sci. Instrum.* **76**(6), 061101 (2005).
- <sup>9</sup>B. Ilic, Y. Yang, and H. G. Craighead, "Virus detection using nanoelectromechanical devices," *Appl. Phys. Lett.* **85**(13), 2604 (2004).
- <sup>10</sup>J. W. Noh, R. Anderson, S. Kim, J. Cardenas, and G. P. Nordin, "In-plane photonic transduction of silicon-on-insulator microcantilevers," *Opt. Express* **16**(16), 12114–12123 (2008).
- <sup>11</sup>D. P. Kelly, M. W. Pruessner, K. Amarnath, M. Datta, S. Kanakaraju, L. C. Calhoun, and R. Ghodssi, "Monolithic suspended optical waveguides for InP MEMS," *IEEE Photonics Technol. Lett.* **16**(5), 1298–1300 (2004).
- <sup>12</sup>N. Siwak, D. Hines, S. Kanakaraju, N. Goldsman, and R. Ghodssi, "Indium phosphide MEMS cantilever resonator sensors utilizing a pentacene absorption layer," *J. Microelectromech. Syst.* **18**(1), 103–110 (2009).
- <sup>13</sup>F. Jiang, A. Keating, M. Martyniuk, R. Pratap, L. Faraone, and J. M. Dell, "Process control of cantilever deflection for sensor application based on optical waveguides," *J. Microelectromech. Syst.* **22**(3), 569–579 (2013).
- <sup>14</sup>M. W. Pruessner, N. Siwak, K. Amarnath, S. Kanakaraju, W.-H. Chuang, and R. Ghodssi, "End-coupled optical waveguide MEMS devices in the indium phosphide material system," *J. Micromech. Microeng.* **16**(4), 832–842 (2006).
- <sup>15</sup>H. Hosaka, K. Itao, and S. Kuroda, "Damping characteristics of beam-shaped micro-oscillators," *Sens. Actuators, A* **49**(1–2), 87–95 (1995).
- <sup>16</sup>N. Emeis, M. Schier, L. Hoffmann, H. Heinecke, and B. Baur, "High speed waveguide-integrated photodiodes grown by metal organic molecular beam epitaxy," *Electron. Lett.* **28**(4), 344–345 (1992).
- <sup>17</sup>M. Pruessner, T. T. King, D. P. Kelly, R. Grover, L. C. Calhoun, and R. Ghodssi, "Mechanical property measurement of InP-based MEMS for optical communications," *Sens. Actuators, A* **105**(2), 190–200 (2003).
- <sup>18</sup>R. Grover, J. V. Hryniewicz, O. S. King, and V. Van, "Process development of methane-hydrogen-argon-based deep dry etching of InP for high aspect-ratio structures with vertical facet-quality sidewalls," *J. Vac. Sci. Technol., B* **19**(5), 1694 (2001).
- <sup>19</sup>M. R. Ravi, A. DasGupta, and N. DasGupta, "Effect of sulfur passivation and polyimide capping on InGaAs-InP PIN photodetectors," *IEEE Trans. Electron Devices* **50**(2), 532–534 (2003).